International Journal of Heat and Mass Transfer 51 (2008) 5785–5793

Contents lists available at ScienceDirect

International Journal of Heat and Mass Transfer

journal homepage: www.elsevier.com/locate/ijhmt

Mixed convection analysis of laminar pulsating flow and heat transfer over a backward-facing step

Khalil Khanafer [a], Bader Al-Azmi [b], Awadh Al-Shammari [c], Ioan Pop [d,*]

[a] Vascular Mechanics Laboratory, Department of Biomedical Engineering, University of Michigan, Ann Arbor, MI 48109, United States
[b] Mechanical Engineering Department, Kuwait University, Al-Safat 13060, Kuwait
[c] Kuwait Air Force Institution, P.O. Box 40204, Al-Jahra 01753, Kuwait
[d] Faculty of Mathematics, University of Cluj, R-3400 Cluj, Romania

ARTICLE INFO

Article history:
Received 22 April 2008
Available online 12 July 2008

ABSTRACT

The present study analyzes mixed convection of laminar pulsatile flow and heat transfer past a backward-facing step in a channel. Discretization of the governing equations was achieved through a finite element scheme based on the Galerkin method of weighted residuals. Temporal variations of streamlines, isotherms, and dimensionless skin friction coefficient and Nusselt number were presented for various relevant dimensionless groups. Fluid flow and heat transfer characteristics were examined in the domain of the Reynolds number, Richardson number and the dimensionless oscillation frequency such that: $100 \leqslant Re \leqslant 1000$, $1.78 \times 10^{-3} \leqslant Ri \leqslant 10$, and $0.1 \leqslant \varpi \leqslant 5$. The working fluid is assigned a Prandtl number of 0.71 throughout this investigation. Our results illustrates that Reynolds number, Richardson number, and dimensionless oscillation frequency have a profound effect on the structure of fluid flow, heat transfer fields, and skin friction coefficient.

1. Introduction

The separation of the flow and its subsequent reattachment to a solid surface has received considerable attention in the literature. This interest stems from its importance in many engineering applications such as internal flow systems (e.g. diffusers, combustors) and flows around airfoils and buildings [1–3]. Of internal separated flows, the backward-facing step flow is the most frequently selected test case for numerical methods due to its geometrical simplicity [4–8]. Armaly et al. [4] conducted a comprehensive experimental and numerical study of backward-facing step flow for a laminar, transitional and turbulent flow of air in a Reynolds number range of $70 < Re < 8000$. Lin et al. [5] analyzed numerically mixed convective heat transfer results for laminar, buoyancy-assisting, two-dimensional flow in a vertical duct with a backward-facing step for a wide range of inlet flow and wall temperature conditions. The authors presented in their work the velocity and temperature distributions along with Nusselt numbers and wall skin friction coefficient for wide ranges of flow and temperature parameters. Mixed convection heat transfer in channels with a heated curved surface bounded by a vertical adiabatic wall was studied numerically by Moukalled et al. [9] for various curvature ratios. Two cases were considered in their work: in the first case, the flow experienced a convex curvature and an increasing cross-sectional flow area (adverse pressure gradient), while in the second case, the flow experienced a concave curvature with a decreasing flow cross-section (favorable pressure gradient). The authors illustrated that for channels with concave walls, where the decrease in cross-sectional area and buoyancy both accelerate the flow, separation was not observed, and considerably greater heat transfer rates were obtained. The overall heat transfer on the concave surface was always greater than a straight channel of equal height. Abu-Mulaweh et al. [10] reported measurements of buoyancy-assisting, laminar mixed convection flow of air along a two-dimensional, vertical backward-facing step. Thereafter, Abu-Mulaweh et al. [11] investigated experimentally laminar mixed convection behind a two-dimensional backward-facing step for the buoyancy-opposing case.

Several numerical simulations of turbulent flow over a backward-facing step were also conducted [1,4,12–18]. Abu-Mulaweh et al. [14] reported measurements of turbulent mixed convection flow over a two-dimensional, vertical backward-facing step using laser-Doppler velocimeter (LDV) and cold wire anemometer, respectively. The effect of the backward-facing step heights on turbulent mixed convection flow along a vertical flat plate was examined by the same authors [15]. It was found that both the reattachment length and the heat transfer rate from the downstream heated wall increased with increasing step height. Several studies were also conducted to analyze the effect of oscillatory flow on the velocity profile and heat transfer characteristics either in a pipe [19–25] or in a channel [26]. However, pulsatile flow and heat transfer characteristics in a channel with a backward-facing

* Corresponding author. Tel.: +40 264 594 315; fax: +40 264 591 906.
E-mail address: pop.ioan@yahoo.co.uk (I. Pop).

0017-9310/$ - see front matter © 2008 Elsevier Ltd. All rights reserved.
doi:10.1016/j.ijheatmasstransfer.2008.04.060

Nomenclature

C_f	dimensionless skin friction coefficient
$\overline{C}_f$	average skin friction coefficient
g	acceleration due to gravity
Gr	Grashof number, $g\beta\Delta T H^3/\nu^2$
h	height of the upstream of the channel
H	height of the step
k	thermal conductivity
Nu	local Nusselt number
$\overline{Nu}$	average Nusselt number
p	pressure
P	dimensionless pressure, $p/(\rho U_o^2)$
Pr	Prandtl number, ν/α
Re	Reynolds number, $U_o H/\nu$
Ri	Richardson number, Gr/Re^2
t	time
T	temperature
T_C	temperature of the cold surface
T_H	temperature of the hot surface
$\mathbf{v}$	dimensional velocity vector
U_o	average velocity upstream of the channel
$\mathbf{V}$	dimensionless velocity vector, $\mathbf{v}/U_o$
x	x-coordinate
X, Y	dimensionless coordinate, $(x, y)/H$
y	y-coordinate

Greek symbols

α	thermal diffusivity
β	coefficient of thermal expansion
ν	kinematic viscosity
ϖ	non-dimensional frequency, $\omega H/U_o$
θ	dimensionless temperature, $(T - T_C)/(T_H - T_C)$
ρ	density
τ	dimensionless time, tU_o/H
τ_w	shear stress

step has received less attention in the literature. Valencia and Hinojosa [27] analyzed numerically incompressible flow of air and heat transfer in a channel with a backward-facing step assuming pulsatile inlet velocity condition and neglecting the effect of the buoyancy force. Their results showed that the wall shear rate in the separation zone varied significantly with pulsatile flow while the heat transfer rate remained relatively constant.

The work by Valencia and Hinojosa [27] did not consider the physics of flow and heat transfer characteristics in depth. Therefore, the objective of the present work was focused on a thorough analysis of the fluid flow and heat transfer in a channel with a backward-facing step under pulsatile flow conditions. In addition, the undergoing investigation examined the effects of pertinent dimensionless parameters on the flow and heat transfer characteristics in the annulus. These parameters are the Richardson number, the amplitude of the velocity, expansion ratio, and Prandtl number. Finally, the implications of the above dimensionless parameters were also depicted on the dimensionless local heat flux and the global Nusselt number predictions.

2. Mathematical formulation

The treated problem is a two-dimensional, transient, laminar convective flow in a channel with a backward-facing step. The physical system considered in the present study is displayed in Fig. 1. The quantities h and H, respectively denote the height of the upstream channel and the step height and have been selected ($h/H = 0.5$) to allow direct validation of the numerical results. The adopted downstream channel length of $30H$ was verified to be sufficient so that the recirculation zone length downstream of the step was independent of the length of the computational domain for all steady and pulsatile flow simulations. The straight wall of the channel is maintained at a uniform temperature that is equal to the inlet air temperature T_C while the stepped wall downstream of the step is heated to a uniform temperature T_H. Under all circumstances $T_H > T_C$ condition is maintained. The upstream portion of the stepped wall and the backward-facing step are treated in this study as adiabatic walls. Furthermore, viscous heat dissipation in the fluid is assumed to be negligible in comparison to conduction and convection heat transfer effects. Also, it is assumed in the undergoing analyses that the thermophysical properties of the fluid are independent of temperature except for the density in the buoyancy term, which is treated according to the Boussinesq approximation.

By incorporating the above points, the system of the governing equations can be expressed in vectorial form as

$$\text{Continuity equation}: \nabla \cdot \boldsymbol{V} = 0 \tag{1}$$

$$\text{Momentum equation}: \frac{\partial \boldsymbol{V}}{\partial \tau} + \boldsymbol{V} \cdot \nabla \boldsymbol{V} = -\nabla P + \frac{1}{Re}\nabla^2 \boldsymbol{V} + \frac{Gr}{Re^2}\theta \tag{2}$$

$$\text{Energy equation}: \frac{\partial \theta}{\partial \tau} + \boldsymbol{V} \cdot \nabla \theta = \frac{1}{PrRe}\nabla^2 \theta \tag{3}$$

The above equations were normalized using the following dimensionless parameters:

$$\boldsymbol{V} = \frac{\mathbf{v}}{U_o},\ P = \frac{P}{\rho U_o^2},\ \tau = \frac{tU_o}{H},\ \theta = \frac{T - T_C}{T_H - T_C},\ (X, Y) = \frac{(x, y)}{H} \tag{4}$$

where P is dimensionless pressure, ρ is the fluid density, $\boldsymbol{V}$ is the dimensionless velocity vector, U_o is the average velocity upstream of the channel, $Re = U_o H/\nu$ is Reynolds number. In addition, the relevant Grashof number and Prandtl number are given by $Gr = g\beta\Delta T H^3/\nu^2$ and $Pr = \nu/\alpha$, respectively.

The boundary conditions for the problem under consideration are expressed as:

1. At the channel inlet, the flow is taken to be unidirectional, pulsating, and at a uniform temperature:
$$U = U_o(1 + \sin \varpi\tau), V = \theta = 0 \tag{5}$$
where ϖ is the non-dimensional frequency $\left(\varpi = \frac{\omega H}{U_o}\right)$.
2. At the exit plane, the gradient of all variables in x-direction were set to zero.

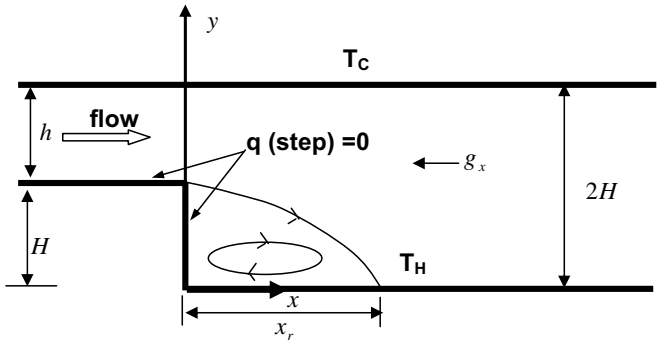

Fig. 1. Schematic diagram of the physical problem.

Table 1
Reattachment lengths for recirculation region in a vertical channel with a backward-facing step ($Re = 100$)

	$Gr = 0$	Error (%)[a]	$Gr = 1000$	Error (%)[a]
Present	**4.99**	0	**3.05**	0
El-Refaee et al. [32]	4.77	4.41	2.99	1.97
Seo and Parameswaran [33]	4.97	0.40	2.95	3.28
Lin et al. [34]	4.91	1.60	3.10	1.64
Chopin [35]	4.61	7.62	2.99	1.97
Hong et al. [36]	4.94	1.00	2.98	2.29
Acharya et al. [37]	4.97	0.40	2.97	2.62
Dyne et al. [38]	4.89	2.01	2.97	2.62
Choudhury and Woolfe [39]	**4.99**	0	**3.21**	5.25

[a] Error relative to the present value.

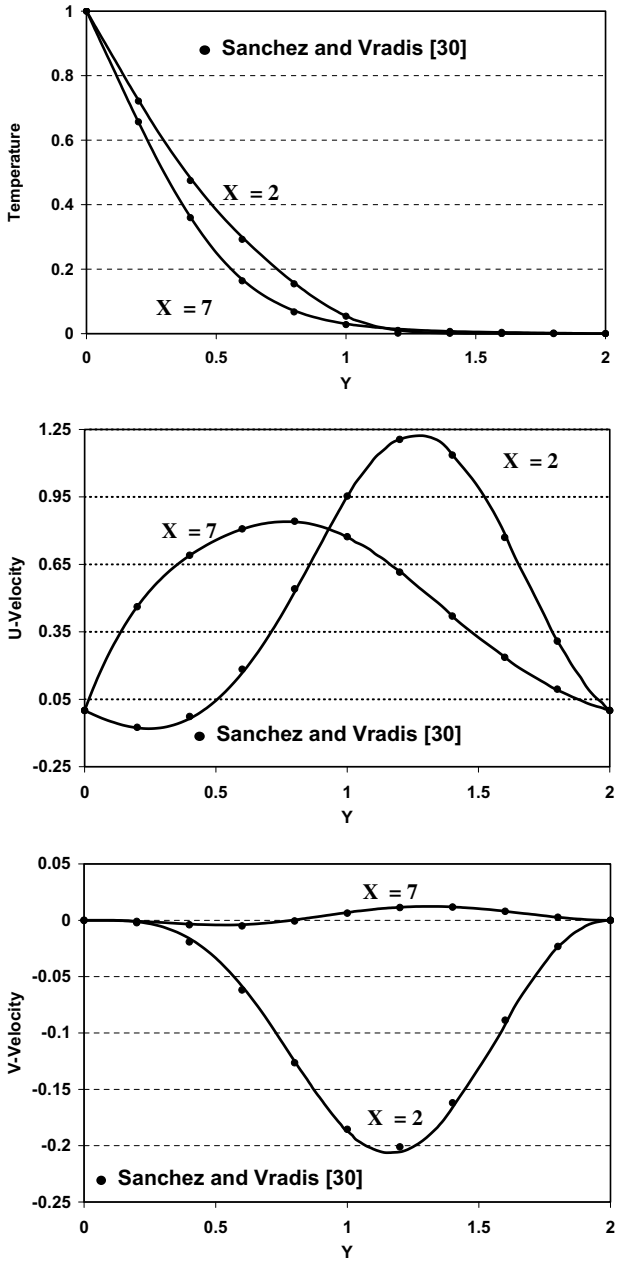

Fig. 2. Comparison of the temperature and velocity profiles between the present study and that of Sanchez and Vradis [30] in a vertical backward facing step ($Re = 100, Ri = 0.1$).

3. The walls are treated as no-slip with a constant temperature. The straight wall was maintained at a constant temperature equal to the uniform inlet temperature, T_C, while the wall downstream of the step was maintained at a uniform temperature, T_H such that $T_H > T_C$. The two walls forming the step were assumed adiabatic as shown in Fig. 1.

Two important dimensionless parameters were determined in this study. The wall shear stress and the heat transfer coefficients were presented in terms of skin friction coefficient and Nusselt number respectively. The local Nusselt number in the channel downstream of the step is defined by

$$Nu_x = \frac{h_x H}{k} = \frac{q_w H}{k(T_H - T_C)} = -\frac{\partial\theta}{\partial Y}\Big|_{Y=0} \tag{6}$$

The dimensionless skin friction coefficient is defined by

$$C_f Re = \frac{\tau_w}{1/2\rho U_o^2} Re = \frac{\mu(\partial u/\partial y)|_{y=0}}{1/2\rho U_o^2} Re = 2\frac{\partial U}{\partial Y}\Big|_{Y=0} \tag{7}$$

Therefore, the average skin friction coefficient is defined as

$$\overline{C}_f Re = \frac{1}{L/H}\int_0^{L/H}\left(2\frac{\partial U}{\partial Y}\Big|_{Y=0}\right)dX \tag{8}$$

3. Numerical scheme

A finite element formulation based on the Galerkin method was utilized to solve the governing equations. The application of this technique is well documented by Taylor and Hood [28] and Gresho et al. [29]. In the current investigation, the continuum domain was divided into a set of non-overlapping regions called elements. Nine

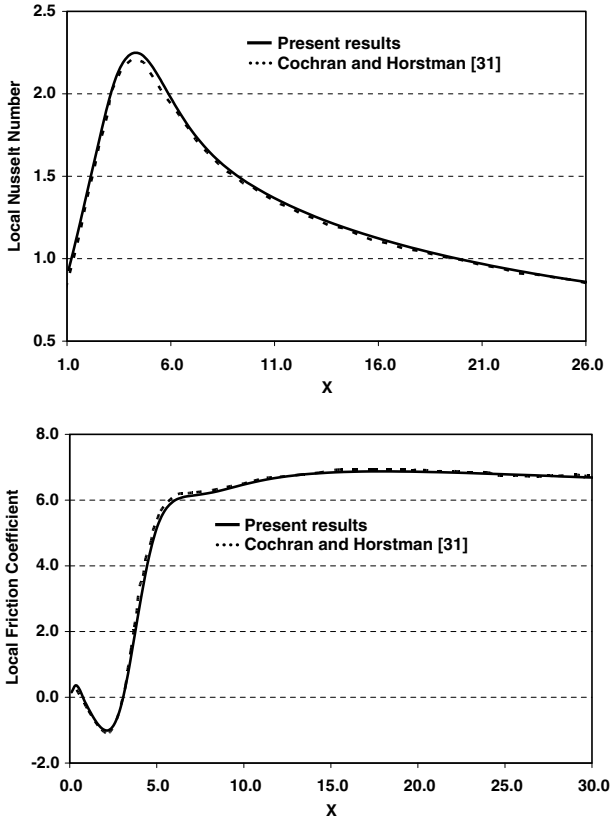

Fig. 3. Comparison of local Nusselt number and local friction coefficient along the heated wall of the backward-facing step between present results and finite element results of Cochran and Horstman [31]. ($Ri = 0.1$, $Re = 100$, $Pr = 0.71$).

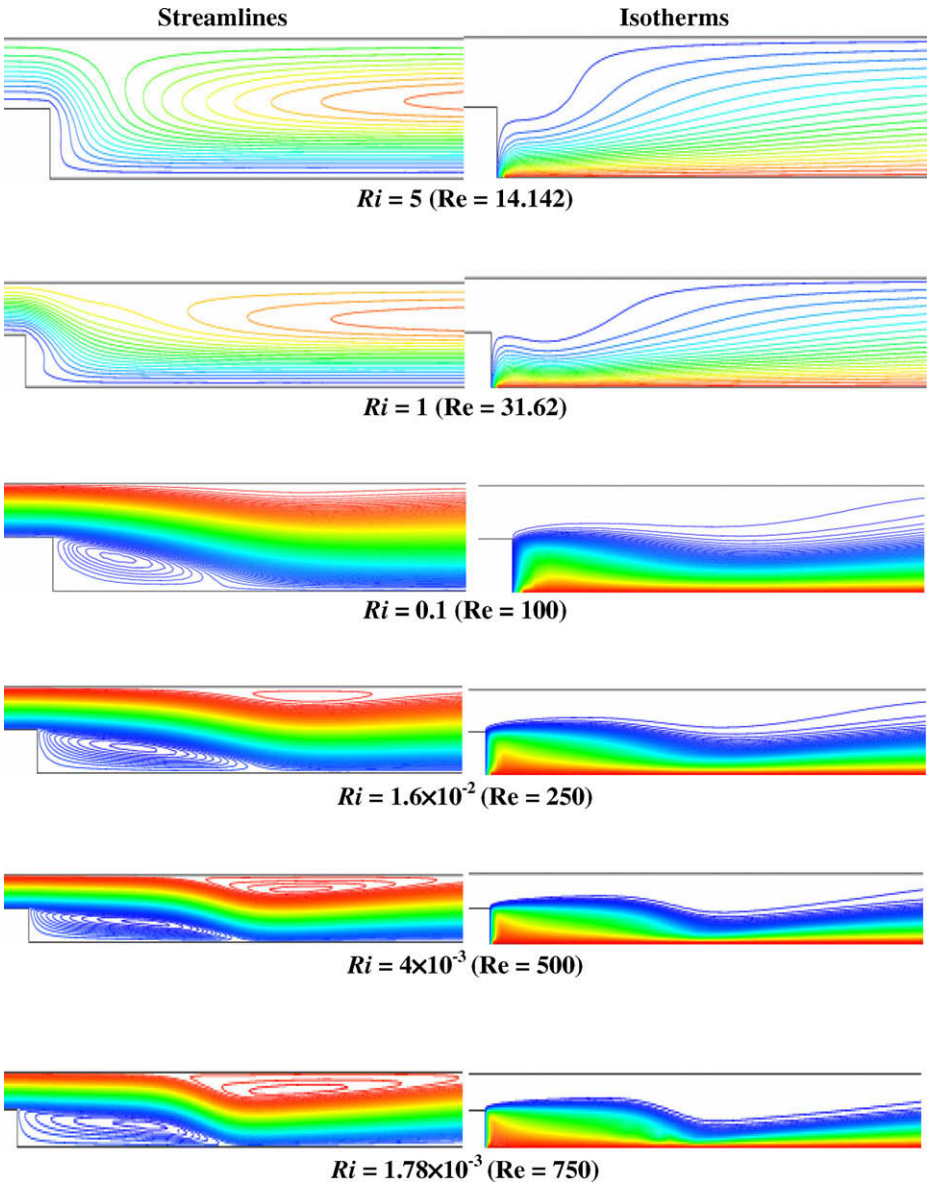

Fig. 4. Effect of Richardson number on the streamlines and isotherms ($Pr = 0.71$).

node quadrilateral elements with bi-quadratic interpolation functions were utilized to discretize the physical domain. Moreover, interpolation functions in terms of local normalized element coordinates were implemented to approximate the dependent variables within each element. Subsequently, substitution of the approximations into the system of the governing equations and boundary conditions yielded a residual for each of the conservation equations. These residuals were then reduced to zero in a weighted sense over each element volume using Galerkin method.

The highly coupled and non-linear algebraic equations resulting from the discretization of the governing equations were solved using an iterative solution scheme called the segregated-solution algorithm. The advantage of using this method lies in that the global system matrix is decomposed into smaller submatrices and then solved in a sequential manner. This technique results in considerably fewer storage requirements. A pressure projection algorithm was utilized to obtain a solution for the velocity field at every iteration step. Furthermore, the pressure projection version of the segregated algorithm was used to solve the non-linear system. In addition, the conjugate residual scheme was used to solve the symmetric pressure-type equation systems, while the conjugate gradient squared method was used for the non-symmetric advection-diffusion-type equations.

Many numerical experiments of various mesh sizes were performed to achieve grid-independent results and to determine the best compromise between accuracy and minimizing computer execution time. As such, a variable grid-size system was employed in this work to capture the rapid changes in the dependent variables especially near the wall where the major gradients occur inside the boundary layer. In order to resolve the large velocity gradients within the recirculation region downstream of the step, the mesh was made finer near the step and in the vicinity of the walls. The solution was advanced in time until periodic convergence solution is achieved.

4. Validation

The present numerical code was first validated against the benchmarked results of the reattachment lengths for recirculation region in a vertical channel with a backward-facing step at

$Re = 100$ as shown in Table 1. Calculations of forced ($Gr = 0$) and mixed ($Gr = 1000$) convection past an adiabatic backward-facing step with an isothermal surrounding walls were presented in Table 1. This table shows an excellent agreement between the results. An additional check of the present numerical approach, Fig. 2 illustrates a comparison of the temperature and velocity profiles at different section of the backward-facing step between the present results and that of Sanchez and Vradis [30]. An excellent agreement was found between both results. Moreover, the results of the present code was validated against local Nusselt number and local skin friction coefficient variations calculated along the heated wall of Cochran and Horstman [31] as depicted in Fig. 3. Fig. 3 shows an excellent agreement between both results.

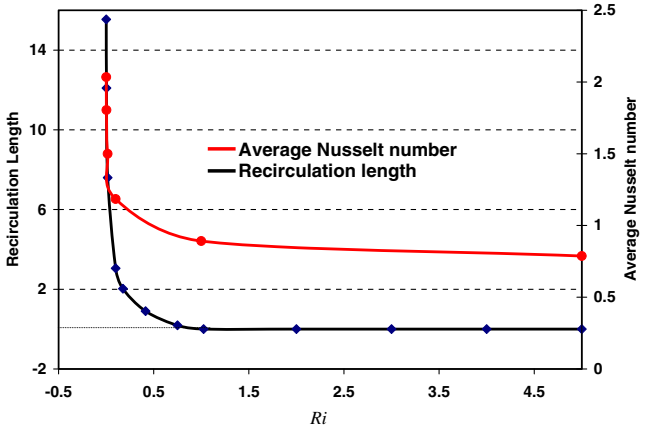

Fig. 5. Effect of Richardson number on the recirculation length and the average Nusselt number along the heated wall for steady flow ($Gr = 1000$, $Pr = 0.71$).

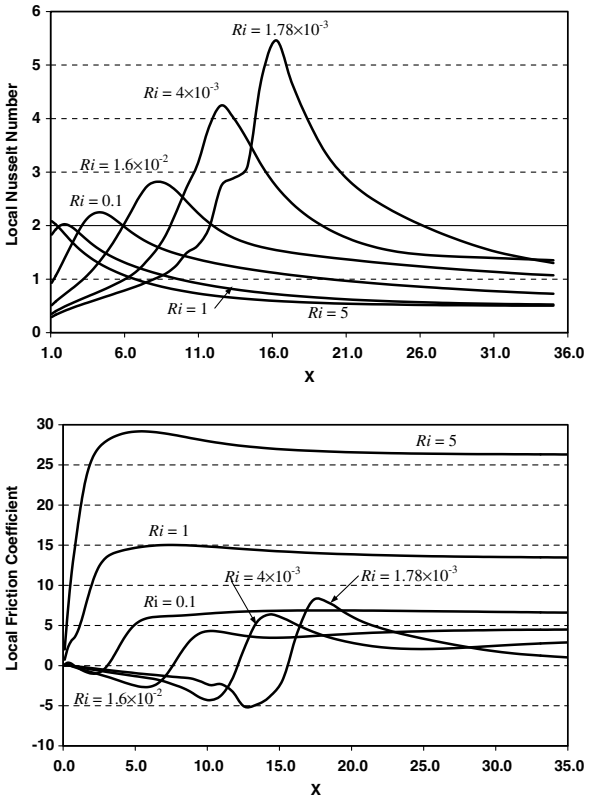

Fig. 6. Effect of Richardson number on the local Nusselt number and local friction coefficient variations along the heated wall ($Gr = 1000$, $Pr = 0.71$).

5. Results and discussion

As stated earlier, the overall objective of the current investigation is to explore time dependent laminar mixed convection heat transfer in a backward-facing step. The implications of varying Reynolds number, Richardson number and the dimensionless oscillation frequency will be emphasized. The results are presented in terms of the temporal variation of the streamline and isotherm patterns. What is more, the temporal variations of the average Nusselt number and skin friction coefficient are highlighted. The Reynolds number is varied between 100 and 1000. In addition, the domain of Richardson number is $1.78 \times 10^{-3} \leqslant Ri \leqslant 10$ and dimensionless oscillation frequency is varied in the range of $0.1 \leqslant \varpi \leqslant 5$.

5.1. Steady case

Steady-state results are first illustrated in the present investigation to show the effect of Richardson number on the streamlines, isotherms, and local variations of skin friction coefficient and Nusselt number as depicted in Figs. 4–6. Fig. 4 demonstrates the steady-state results of the streamlines and isotherms for the range of the Richardson number studied. The Richardson number ($Ri = Gr/Re^2$) gives an indication on the influence of buoyancy force in a forced convection flow. It can be seen from this figure that large Richardson numbers ($Ri \gg 1$) cause the separation near the step to disappear due to the acceleration of the flow near the heated wall. This elimination of the separation region occurs for $Ri > 0.1$.

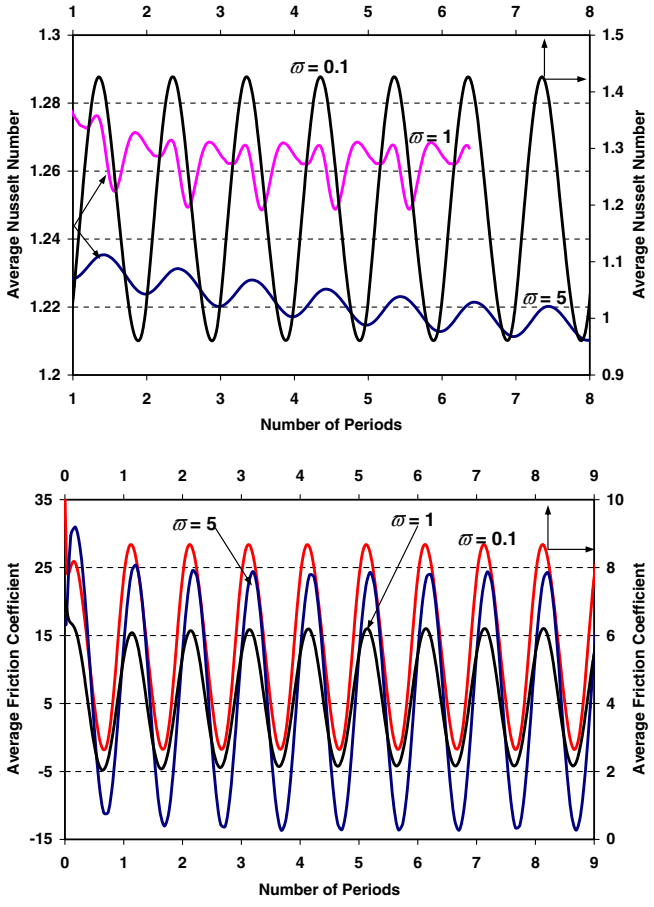

Fig. 7. Effect of dimensionless oscillation frequency on the temporal variations of the average Nusselt number and average friction coefficient for $Re = 100$, $Ri = 0.1$, and $Pr = 0.71$.

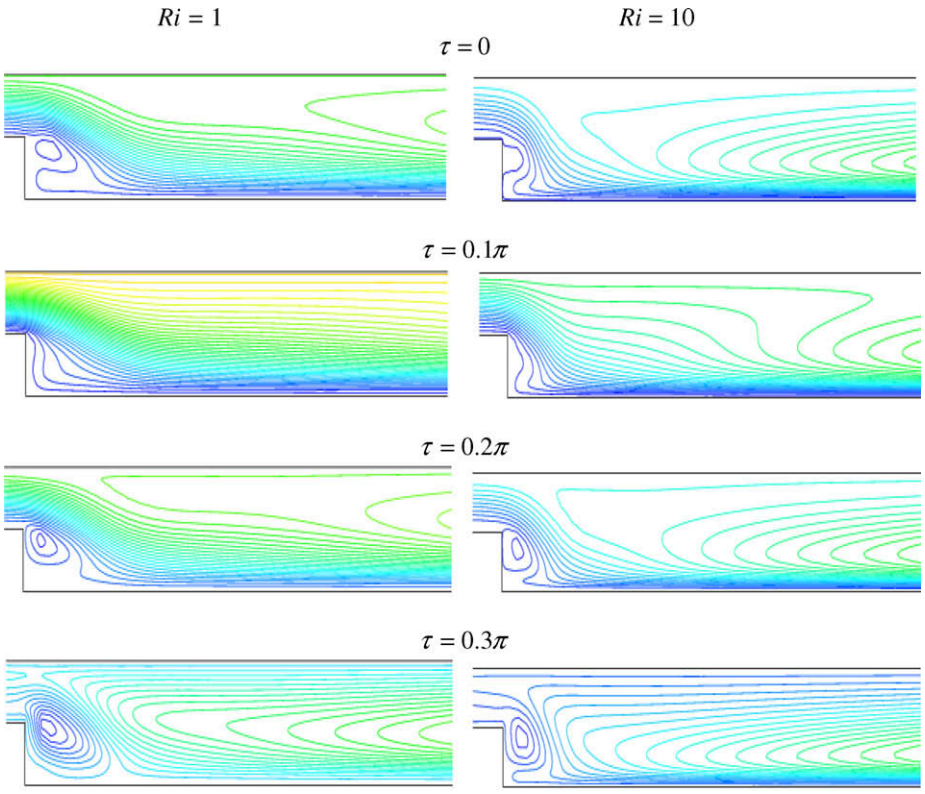

Fig. 8. Effect of Richardson number on the temporal variations of the streamlines ($Re = 100$, $\varpi = 5$, $Pr = 0.71$).

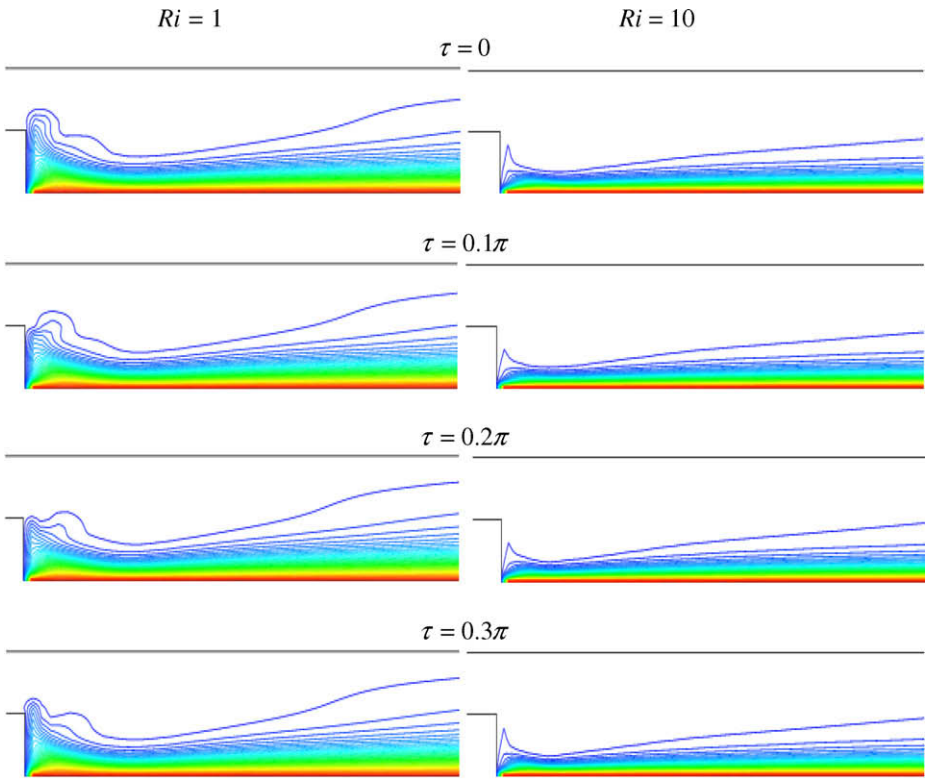

Fig. 9. Effect of Grashof number on the temporal variations of the isotherms ($Re = 100$, $\varpi = 5$, $Pr = 0.71$).

However, as Reynolds number increases (or decrease Richardson number), the impact of forced convection is observed and the recirculation zone along the heated surface becomes larger as evident in Fig. 4. As *Re* is raised to 750, a further increase in the size of

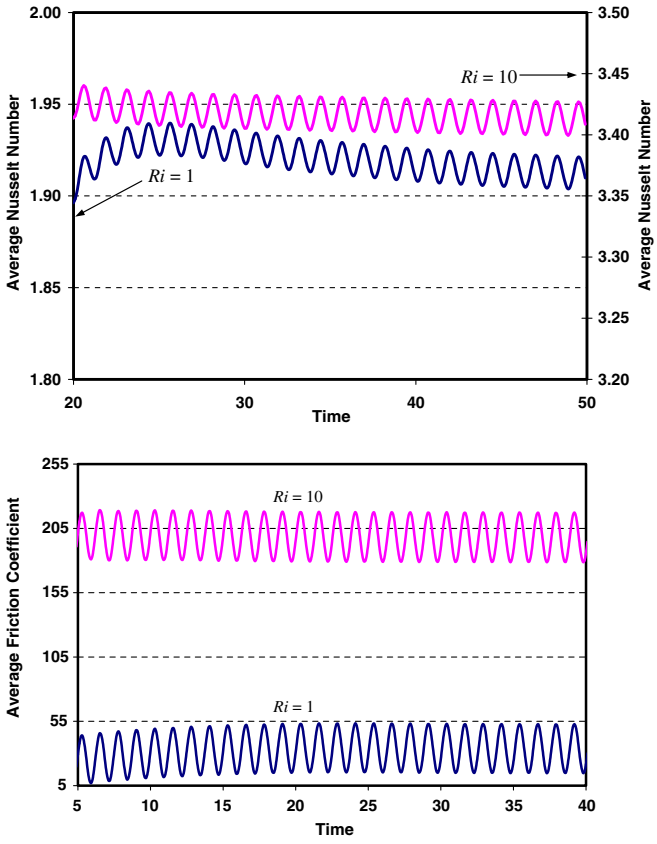

Fig. 10. Effect of Richardson number on the temporal variations of the average Nusselt number and average friction coefficient for $Re = 100$, $\varpi = 5$, and $Pr = 0.71$.

the recirculation region is exhibited. The stronger separation at the higher Re is due to the higher adverse pressure gradients associated with the area expansion in the channel. As such, for low Richardson number ($Ri \ll 1$), the buoyancy effect can be neglected, and separation occurs near the step end. At higher Re values ($Re \geqslant 500$), Fig. 4 illustrates that the separation adjacent to the cold horizontal surface becomes larger. The corresponding isotherm plots for the above cases are presented in Fig. 4. The thermal boundary layer decreases in thickness as Reynolds number increases (or decrease Richardson number) and consequently increases the heat transfer rate. The impact of Richardson number on the average Nusselt number and the length of recirculation zone is depicted in Fig. 5. Both parameters decrease with an increase in Richardson number.

The effect of Richardson number on the local variations of Nusselt number and skin friction coefficient is illustrated in Fig. 6. It is noticed that peak values of the Nusselt number are found near the reattachment points. Moreover, as Richardson number decreases (increases Re), the local variation of Nusselt number increases within the recirculation region as well as the region right after the recirculation bubble. Fig. 6 shows that the dimensionless local variation of skin friction coefficient along the heated wall is higher for the case of $Ri = 5$ because of high velocity near the heated wall due to the buoyant effect. The buoyancy force increases the velocity gradient near the heated wall and consequently increases the wall skin friction coefficient. For $Ri > 0.1$, the friction coefficient remains positive throughout the entire length of the heated wall. This is due to the absence of the recirculation bubble along the heated wall.

5.2. Transient case

The aim of this section is to provide an insight into the effects of various pertinent parameters on the temporal variations of flow structures, isotherms, average Nusselt number, and average wall friction coefficient. The effect of the dimensionless oscillation frequency (ϖ) on the temporal variations of the average Nusselt number and average friction coefficient are presented in Fig. 7 for $Re = 100$ and $Ri = 0.1$. This figure illustrates how quickly the steady periodic solution is reached for various ϖ. The steady periodic solution reaches quicker for large ϖ as depicted in Fig. 7. However, for a small frequency ($\varpi = 0.1$), small number of periods (or large time) is required to reach a steady-periodic solution as demonstrated in Fig. 7. It is interesting to note that when the normalized

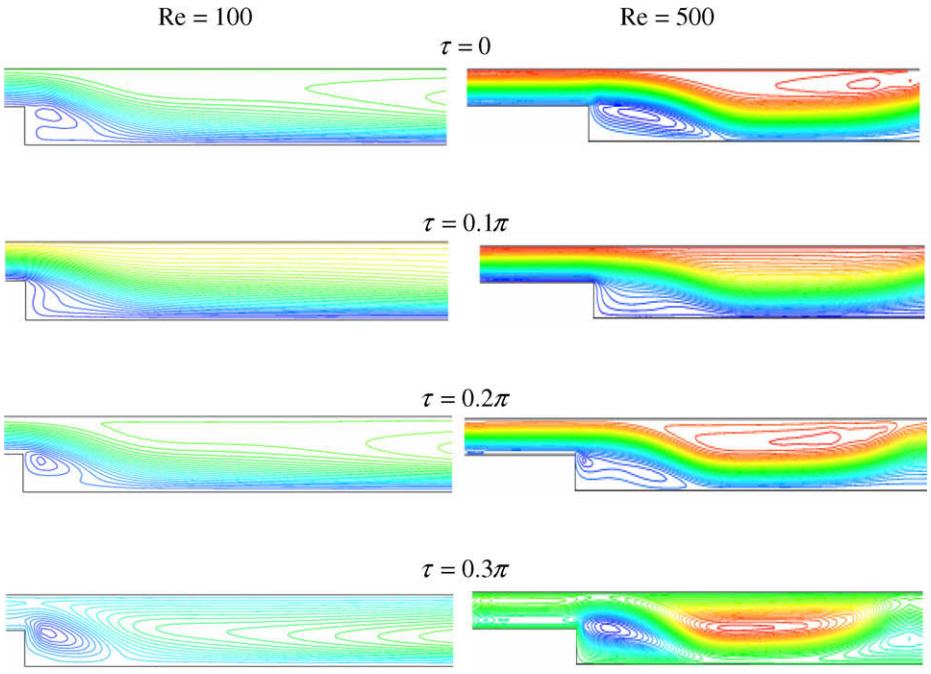

Fig. 11. Effect of Reynolds number on the temporal variations of the streamlines ($Gr = 10^4$, $\varpi = 5$, $Pr = 0.71$).

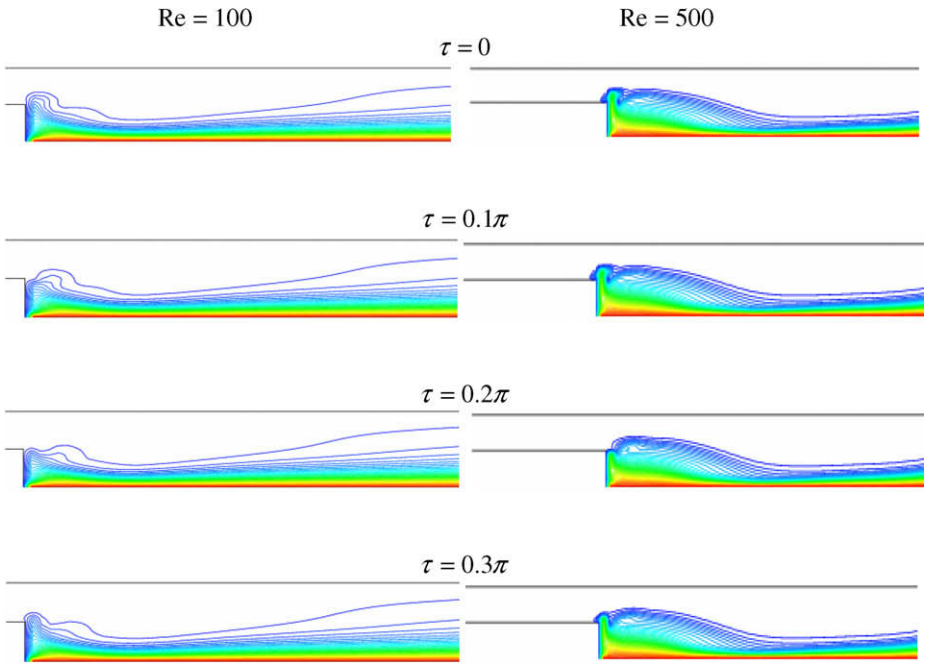

Fig. 12. Effect of Reynolds number on the temporal variations of the isotherms ($Gr = 10^4$, $\varpi = 5$, $Pr = 0.71$).

frequency is relatively small, as seen in Fig. 7, the augmentation of convective heat transfer is apparent at this condition. This is clearly reflected on the magnitude of the calculated Nusselt numbers. Fig. 7 also demonstrates the temporal variation of the average friction coefficient at three different dimensionless frequencies. The results show that an elevation in the frequency value brings about an increase in the magnitude of the friction coefficient. Furthermore, it is noticed that the friction coefficient follows a sinusoidal oscillation pattern.

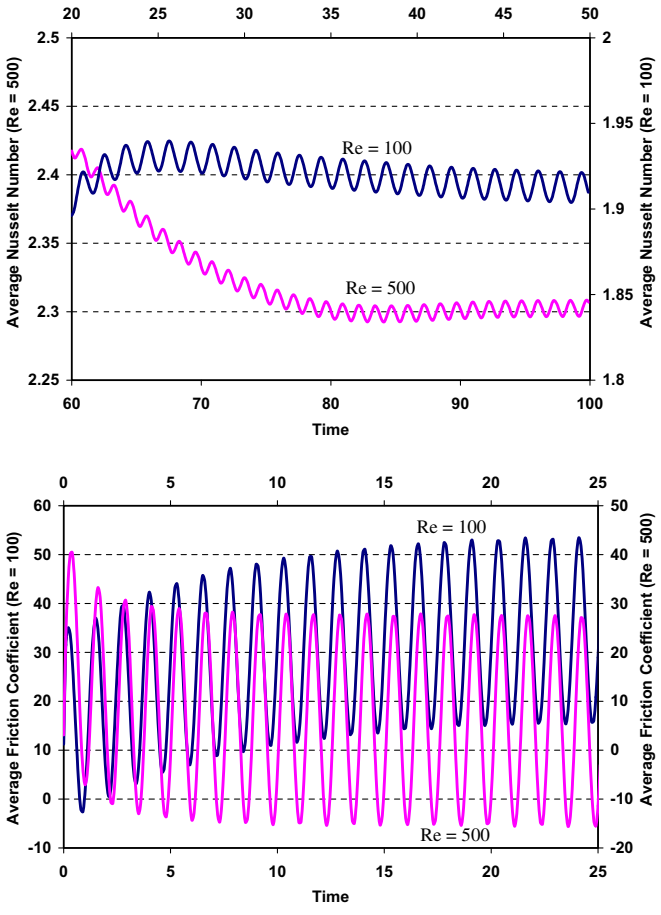

Fig. 13. Effect of Reynolds number on the temporal variations of the average Nusselt number and average friction coefficient for $Gr = 10^4$, $\varpi = 5$, and $Pr = 0.71$.

The sensitivity of the streamline and isotherm patterns due to the variation in Richardson number is presented in Figs. 8 and 9 for $Re = 100$ and $\varpi = 5$. The results in Figs. 8 and 9 are presented when the solution reached the steady-periodic flow condition. As Richardson number increases, the intensity of convection intensifies within the cavity due to the increase in buoyancy effect. This is evident from the substantial decrease in the boundary layer thickness along the heated wall. At the beginning of the cycle, Fig. 8 shows a vortex at he upper corner of step plane. The size of this vortex is smaller for high Richardson number ($Ri = 10$). As the flow accelerates through the channel, this vortex disappears as depicted in Fig. 8. At peak flow condition, the flow is essentially a potential flow for $Ri = 1$. However, for high Richardson number ($Ri = 10$), a central vortex occupies most of the channel. During the positive deceleration phase of the cycle, a large vortex exists at the upper corner of the step and its size grows and become clearly visible at the maximum negative oscillating speed ($\tau = 0.3\pi$). At this condition, the channel is completely filled by a central vortex except at the corner of the step. The computed isotherms in Fig. 9 are qualitatively similar, but the thermal boundary layer for the case with high Richardson number ($Ri = 10$) is thinner than those with lower Richardson number ($Ri = 1$). The effect of Richardson number on the temporal variations of the average Nusselt number and average friction coefficient for $Re = 100$ and $\varpi = 5$ is demonstrated in Fig. 10. As Richardson number increases, the convection activities within the channel intensify and, as a result, the average Nusselt number increases along the heated wall. Fig. 10 shows that Richardson number has a significant effect on the average friction coefficient along the heated wall for $Re = 100$ and $\varpi = 5$. This figure illustrates that the average friction coefficient is substantially higher for $Ri = 10$ than for $Ri = 1$ because of high velocity gradient near the heated wall.

Next, Figs. 11–13 illustrate the impact of Re on the temporal variation of the streamlines, isotherms, average Nusselt number, and average friction coefficient for $Ri = 1$ and $\varpi = 5$. Fig. 11 shows a considerable variation in the flow pattern through the pulsatile cycle. At the onset of the cycle, a small vortex is presented at the upper corner of the backward-facing step wall at $Re = 100$ while a large recirculation zone is exhibited at a larger Reynolds number ($Re = 500$) as shown in Fig. 11. As the flow accelerates, Fig. 11 shows that the vortices disappear for both Reynolds number at peak flow condition. During the deceleration phase, the expansion of the vortices in the channel is observed. Fig. 12 illustrates that as Reynolds number increases, the thermal boundary layer along the heated wall decreases and consequently increases the heat transfer characteristics. The effect of the Reynolds number on the temporal variations of the average Nusselt number and average wall friction coefficient is displayed in Fig. 13 for $Ri = 1$ and $\varpi = 5$. The results indicate that as Reynolds number increases, the temporal variation of the average Nusselt number prediction along the heated wall increases. The effect of the Reynolds number on the temporal variation of the average wall friction coefficient is also shown in Fig. 13. It is observed that the average wall skin friction coefficient decreases with an increase in Reynolds number because the buoyancy force decreases with an increase in Reynolds number. As such, the velocity gradients near the heated wall decrease.

6. Conclusions

Mixed convection of pulsating flow and heat transfer characteristics over a backward-facing step under laminar regime was numerically investigated. The investigation was carried out for a number of pertinent dimensionless groups, namely the Reynolds number, Richardson number, and the dimensionless oscillation frequency. The presented results captured the steady-periodic solutions. Such results show that the Reynolds number and Richardson number have a profound effect on the structure of fluid flow and heat transfer fields. The results indicate that the average Nusselt number increases with an increase in both Reynolds and Grashof numbers while decreases with an increase in the oscillation frequency. Moreover, the results illustrated that the average wall friction coefficient increases with an increase in both Richardson number and oscillation frequency whereas decreases with in increase in Reynolds number. Finally, the present numerical results can serve as useful source materials against which the outcome of future analytical and experimental investigations can be checked.

References

[1] H. Le, P. Moin, J. Kim, Direct numerical simulation of turbulent flow over a backward-facing step, J. Fluid Mech. 330 (1997) 349–374.
[2] T. Lee, D. Mateescu, Experimental and numerical investigation of 2D backward-facing step flow, J. Fluids Struct. 12 (1998) 703–716.
[3] O.G. Martynenko, P.P. Khramtsov, Free-Convective Heat Transfer : With Many Photographs of Flows and Heat Exchange, Springer, Berlin, 2005.
[4] B.F. Armaly, F. Durst, J.C.F. Schonung, Experimental and theoretical investigation of backward-facing step flow, J. Fluid Mech. 127 (1983) 473–496.
[5] J.T. Lin, B.F. Armaly, T.S. Chen, Mixed convection in buoyancy-assisting vertical backward-facing step flows, Int. J. Heat Mass Transfer 10 (1990) 2121–2132.
[6] B.J. Baek, B.F. Armaly, T.S. Chen, Measurements in buoyancy-assisting separated flow behind a vertical backward-facing step, J. Heat Transfer 2 (1993) 403–408.
[7] B. Hong, B.F. Armaly, T.S. Chen, Laminar mixed convection in a duct with a backward-facing step – the effects of inclination angle and Prandtl number, Int. J. Heat Mass Transfer 36 (1993) 3059–3067.
[8] H.I. Abu-Mulaweh, B.F. Armaly, T.S. Chen, Laminar natural convection flow over a vertical backward-facing step, J. Heat Transfer 117 (1995) 895–901.
[9] F. Moukalled, A. Doughan, S. Acharya, Parametric study of mixed convection in channels with concave and convex surfaces, Int. J. Heat Mass Transfer 43 (2000) 1947–1963.
[10] H.I. Abu-Mulaweh, B.F. Aramaly, T.S. Chen, Effects of upstream wall heating on mixed convection in separated flows, J. Thermophys. Heat Transfer 9 (1995) 715–721.
[11] H.I. Abu-Mulaweh, B.F. Aramaly, T.S. Chen, Measurements in buoyancy-opposing Laminar flow over a vertical backward-facing step, J. Heat Transfer 116 (1994) 247–250.
[12] F. Durst, J.C.F. Pereira, Time-dependent Laminar backward-facing step flow in a two dimensional duct, Trans. ASME J. Fluids Engng. 110 (1988) 289–296.
[13] L. Kaiktsis, G.E. Karnniadakis, S.A. Orszag, Onset of three-dimensionality, equilibria, and early transition in flow over a backward-facing step, J. Fluid Mech. 231 (1991) 501–528.
[14] H.I. Abu-Mulaweh, B.F. Armaly, T.S. Chen, Turbulent mixed convection flow over a backward-facing step, Int. J. Heat Mass Transfer 44 (2001) 2661–2669.
[15] H.I. Abu-Mulaweh, T.S. Chen, B.F. Armaly, Turbulent mixed convection flow over a backward-facing step – the effect of the step heights, Int. J. Heat Fluid Flow 23 (2002) 758–765.
[16] H.I. Abu-Mulaweh, T.S. Chen, B.F. Armaly, Turbulent natural convection flow over a backward-facing step, Exp. Heat Transfer 12 (1999) 295–308.
[17] K. Abe, T. Kondoh, Y. Nagano, A new turbulence model for predicting fluid-flow and heat transfer in separating and reattaching flows. I. Flow field calculations, Int. J. Heat Mass Transfer 37 (1994) 139–151.
[18] K. Abe, T. Kondoh, Y. Nagano, A New turbulence model for predicting fluid-flow and heat transfer in separating and reattaching flows. II. Thermal field calculations, Int. J. Heat Mass Transfer 38 (1995) 1467–1481.
[19] J.R. Womersley, Oscillatory motion of a viscous liquid in a thin walled elastic tube. I. The linear approximation for long waves, Philos. Mag. 46 (1955) 199–221.
[20] S. Uchida, The pulsating viscous flow superimposed on the steady Laminar motion of incompressible fluid in a circular pipe, Z. Angew. Math. Phys. 7 (1956) 403–422.
[21] H.B. Atabek, C.C. Chang, Oscillatory flow near the entry of a circular tube, Z. Angew. Math. Phys. 112 (1961) 185–201.
[22] H.B. Atabek, C.C. Chang, L.M. Fingerson, Measurement of Laminar oscillatory flow in the inlet length of a circular tube, Phys. Med. Biol. 9 (1964) 219–227.
[23] R. Siegel, M. Perlmutter, Heat transfer for pulsating Laminar duct Flow, ASME J. Heat Transfer 8 (1962) 111–116.
[24] H.W. Cho, J.M. Hyun, Numerical solutions of pulsating flow and heat transfer characteristics in a pipe, Int. J. Heat Fluid Flow 11 (1990) 321–330.
[25] K.M. Khanafer, J.L. Bull, I. Pop, R. Berguer, Influence of pulsatile blood flow and heating scheme on the temperature distribution during hyperthermia treatment, Int. J. Heat Mass Transfer 50 (2007) 4883–4890.
[26] S.Y. Kim, B.H. Kang, J.M. Hyun, Heat transfer in the thermally developing region of a pulsating channel flow, Int. J. Heat Mass Transfer 36 (1993) 4257–4266.
[27] A. Valencia, L. Hinojosa, Numerical solutions of pulsating flow and heat transfer characteristics in a channel with a backward-facing step, Heat Mass Transfer 32 (1997) 143–148.
[28] C. Taylor, P. Hood, A numerical solution of the Navier–Stokes equations using finite-element technique, Comput. Fluids 1 (1973) 73–89.
[29] P.M. Gresho, R.L. Lee, R.L. Sani, On the time-dependent solution of the incompressible Navier–Stokes equations in two and three dimensions, in: Recent Advances in Numerical Methods in Fluids, Pineridge, Swansea, UK, 1980.
[30] J.G. Sanchez, G.C. Vradis, Mixed convection heat transfer over a backward-facing step, in: B.F. Blackwell, B.F. Armally (Eds.), Computational Aspects of Heat Transfer-Benchmark Problems, ASME HTD-258, 1993.
[31] R.J. Cochran, R.H. Horstman, Benchmark solution for a vertical buoyancy-assisted laminar backward-facing step flow using finite element, finite volume and finite difference methods, in: B.F. Blackwell, B.F. Armally (Eds.), Computational Aspects of Heat Transfer-Benchmark Problems, ASME HTD-258, 1993, pp. 37–47.
[32] M.M. El-Refaee, M.M. El-Sayed, N.M. Al-Najem, I.E. Megahid, Steady-state solutions of buoyancy-assisted internal flows using a fast false implicit transient scheme (FITS), Int. J. Numer. Meth. Heat Fluid Flow 6 (1996) 3–23.
[33] E. Seo, S. Parameswaran, Numerical computations of steady and unsteady, separating, buoyant flows. Part I. Computations with the standard $k-\varepsilon$ model, Numer. Heat Transfer A 42 (2002) 791–809.
[34] J.T. Lin, B.F. Armaly, T.S. Chen, Mixed convection in buoyancy-assisted vertical backward-facing step flows, Int. J. Heat Mass Transfer 33 (1990) 2121–2132.
[35] T.R. Chopin, Mixed convection flow and heat transfer in a vertical backward-facing step using FLOTRAN CFD program, in: B.F. Blackwell, B.F. Armally (Eds.), Computational Aspects of Heat Transfer-Benchmark Problems, ASME HTD-258, 1993.
[36] B. Hong, B.F. Armaly, T.S. Chen, Mixed convection in a laminar, vertical, backward-facing step flow, in: B.F. Blackwell, B.F. Armally (Eds.), Computational Aspects of Heat Transfer-Benchmark Problems, ASME HTD-258, 1993.
[37] S. Acharya, G. Dixit, Q. Hou, Laminar mixed convection in a vertical channel with a back-step: a benchmark study, in: B.F. Blackwell, B.F. Armally (Eds.), Computational Aspects of Heat Transfer-Benchmark Problems, ASME HTD-258, 1993.
[38] B.R. Dyne, D.W. Pepper, F.P. Brueckner, Mixed convection in a vertical channel with a backward-facing step, in: B.F. Blackwell, B.F. Armally (Eds.), Computational Aspects of Heat Transfer-Benchmark Problems, ASME HTD-258, 1993.
[39] D. Choudhury, A.E. Woolfe, Computation of laminar forced and mixed convection in a heated vertical duct with a step, in: B.F. Blackwell, B.F. Armally (Eds.), Computational Aspects of Heat Transfer-Benchmark Problems, ASME HTD-258, 1993.